ACS APPLIED MATERIALS & INTERFACES

Research Article

www.acsami.org

Synthesis and Characterization of Ionic Polymer Networks in a Room-Temperature Ionic Liquid

Joseph F. Stanzione, III,[†,‡] Robert E. Jensen,[§] Philip J. Costanzo,[§,⊥] and Giuseppe R. Palmese[†,§]

[†]Department of Chemical & Biological Engineering, Drexel University, Philadelphia, Pennsylvania 19104, United States

[§]Army Research Laboratory, RDRL-WMM-C, Aberdeen Proving Ground, Maryland 21005, United States

ABSTRACT: Ionic liquid gels (ILGs) for potential use in ion transport and separation applications were generated via a free radical copolymerization of 2-acrylamido-2-methyl-1-propanesulfonic acid (AMPS) and *N,N′*-methylene(bis)acrylamide (MBA) using 1-ethyl-3-methylimidazolium ethylsulfate (IL) as a room temperature ionic liquid solvent medium. The AMPS and MBA monomer solubility window in the IL in the temperature range of 25 to 65 °C was determined. *In situ* ATR-FTIR showed near complete conversion of monomers to a cross-linked polymer network. ILGs with glass transition temperatures (T_gs) near −50 °C were generated with T_g decreasing with increasing IL content. The elastic moduli in compression (200 to 6600 kPa) decreased with increasing IL content and increasing AMPS content while the conductivities (0.35 to 2.14 mS cm^{-1}) increased with increasing IL content and decreasing MBA content. The polymer-IL interaction parameter (χ) (0.48 to 0.55) was determined via a modified version of the Bray and Merrill equation.

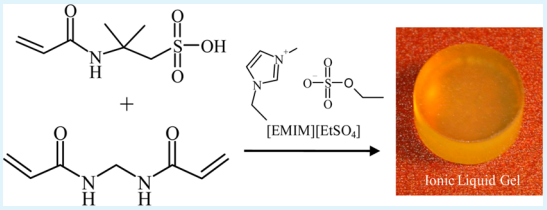

KEYWORDS: *room-temperature ionic liquids, gels, thermosets, polyacrylamides, ion transport*

INTRODUCTION

Room-temperature ionic liquids (RTILs) are ambient temperature molten salts that have gained great attention as advantageous polymerization media, among other unique functions. This is a result of RTILs having low vapor pressures and relatively low viscosities.[1,2] Additionally, they possess good thermal and chemical stability and relatively high ion conductivity, are highly tunable "designer" molecular structures, and are considered environmentally friendly chemicals.[1,2] Numerous research groups have demonstrated the ability to synthesize polymers in RTILs utilizing a variety of traditional monomers. For instance, Hong et al. free radically polymerized styrene and methyl methacrylate in 1-butyl-3-methylimidazolium hexafluorophosphate and Li et al. polymerized methyl methacrylate in *N*-butyl-*N′*-methylimidazolium hexafluorophosphate.[3,4] Additionally, Snedden et al. carried out the polymerizations of methyl methacrylate, styrene, and acrylonitrile in *N,N′*-dialkylimidazolium salts of $[PF_6]^-$, $[BF_4]^-$, $[N(SO_2CF_3)_2]^-$, or $[F(HF)_n]^-$, whereas Strehmel et al. described the free radical polymerization of *n*-butyl methacrylate in an assortment of RTILs.[5,6] One of the RTILs employed in this study was 1-ethyl-3-methylimidazolium ethylsulfate [EMIM]-[$EtSO_4$] whereby *n*-butyl methacrylate was polymerized in situ and tested. Furthermore, Susan et al. described ionic polymer gels of poly(methyl methacrylate) that were free radically polymerized in 1-ethyl-3-methyl imidazolium bis-(trifluoromethane sulfonyl)imide to produce a series of polymer electrolytes.[7] The ability of a number of RTILs that dissolve both monomers and polymers have also been tabulated by Winteron.[8] Lastly, Matsumoto et al. polymerized bisphenol A diglycidyl ether and tetrafunctional epoxy resins with tetraethylenepentamine in the presence of 1-ethyl-3-methylimidazolium bis(trifluoromethane sulfonyl)imide.[9] The compatibility of the polymer network and the ionic liquid was demonstrated to greatly influence the ionic conductivity and ionic confinement of the solvent. In addition, the mechanical strength and morphology of the materials greatly depended on the ionic liquid content.

In this study, ILGs were generated via a free radical copolymerization of 2-acrylamido-2-methyl-1-propanesulfonic acid (AMPS) and *N,N′*-methylene(bis)acrylamide (MBA) using 1-ethyl-3-methylimidazolium ethylsulfate ([EMIM]-[$EtSO_4$]) as a RTIL solvent medium. Because of AMPS and MBA being extensively studied in responsive hydrogel systems and the ability of AMPS to conduct protons via the sulfonic acid moiety as well as possessing excellent solvent uptake and retention properties, AMPS and MBA (Scheme 1) were selected as the monofunctional and bifunctional monomers, respectively, to produce hydrogel-like polymeric materials that incorporate a unique solvent medium.[10−14] Fundamental physical properties of the ILGs such as the glass transition temperature, mechanical modulus, swelling, and ionic conductivity were examined. The intention of this study was to synthesize and characterize polymer gels that contain ionic character not only in the solvent medium but also in the polymer network with the potential to support ion transport and separation applications.

Received: August 24, 2012
Accepted: October 22, 2012
Published: October 22, 2012

Scheme 1. Chemical Structures of AMPS (top left), MBA (top right), [EMIM][EtSO$_4$] (bottom left), and PPS (bottom right)

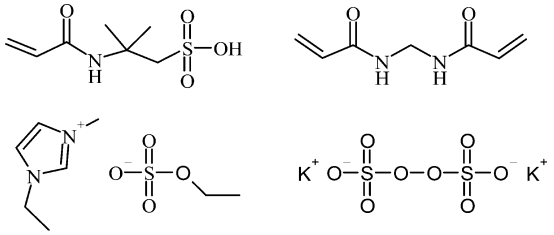

EXPERIMENTAL SECTION

Materials. The chemical structures of 2-acrylamido-2-methyl-1-propanesulfonic acid (AMPS, Sigma Aldrich, 99% purity), *N,N′*-methylene(bis)acrylamide (MBA, Sigma Aldrich, 99% purity), 1-ethyl-3-methylimidazolium ethylsulfate ([EMIM][EtSO$_4$], Fluka, ≥ 95% purity) and potassium persulfate (PPS, Sigma Aldrich, 99.99% purity) are shown in Scheme 1. AMPS, MBA, and PPS are crystalline white solids at room temperature. PPS was used as a free radical initiator. All chemicals were used as received.

Monomer Solubility in [EMIM][EtSO$_4$]. An estimate of the solubility limits of the monomers in [EMIM][EtSO$_4$] was determined using the following procedure. Finely ground AMPS or MBA was added to [EMIM][EtSO$_4$] in concentrations of no more than 0.70 g of monomer per mL of [EMIM][EtSO$_4$] to produce approximately 5 mL solutions. The solutions were conditioned at 130 °C under a partial vacuum pressure of 100 kPa to eliminate residual water. After complete dissolution, the solutions were allowed to cool to room temperature. If visible precipitation of monomer occurred prior to 30 min, the solutions were considered immiscible. Thirty minutes was considered the maximum allowable mixing time window. Solutions that appeared to be close to the solubility limit were further heated to 65 °C in a nitrogen-purged atmosphere and left overnight. If precipitation continued to occur while in the 65 °C oven, then the solution was also considered insoluble. For solutions containing both AMPS and MBA, AMPS was dissolved into [EMIM][EtSO$_4$] first, followed by the MBA under the same temperature and pressure conditions described previously. Again, solubility was determined by the allowable mixing time window.

As defined by the time and temperature constraints of our ILG synthesis procedure, the effective solubility window of AMPS and MBA completely dissolved in [EMIM][EtSO$_4$] is illustrated in Figure 1a as the dashed region on the ternary plot. AMPS and MBA have maximum workable mole fractions (x) of 0.30 and 0.125, respectively, corresponding to points A and D in Figure 1a. The maximum workable combined monomer mole fraction is along the x_{RTIL} = 0.65 line with AMPS having 0.225 ≤ x_{AMPS} ≤ 0.25 and MBA having 0.10 ≤ x_{AMPS} ≤ 0.125, corresponding to points B and C in Figure 1a. Chemical formulations of AMPS and MBA in [EMIM][EtSO$_4$] outside the solubility window exhibited immediate monomer precipitation.

Once the approximate solubility window was known, the properties of the ILGs were probed by either setting x_{MBA}:x_{AMPS} to 0.36 while varying x_{RTIL} from 0.68 to 0.90 (ILGs 1−6) or by setting x_{RTIL} to 0.80, while varying x_{MBA}:x_{AMPS} from 0.20 to 1.10, as shown in Figure 1b. Notice that Figure 1b is a magnified version of the lower right portion of Figure 1a.

ILG Synthesis. All syntheses utilized AMPS, MBA, and PPS in a homogeneous solution with [EMIM][EtSO$_4$] as the solvent medium. Described is the general ILG synthesis procedure. Based on the specified formulation, the appropriate amount of AMPS was completely dissolved into [EMIM][EtSO$_4$] by manually mixing the solution and then subsequently loading it into a 130 °C oven under a continuous negative pressure draw of 100 kPa in 10 min intervals. The appropriate amount of MBA was then dissolved into the solution in the same manner. Upon observable dissolution of the monomers, the solution was cooled to room temperature and PPS was added (one mole of PPS per 35 mols of carbon−carbon double bonds (C═C)). Thereafter, the solution was dispensed into a mold that was then placed in a vacuum oven at 30 °C and evacuated to a negative pressure of 100 kPa until visible outgassing no longer occurred. Next, the vacuum oven was backfilled with nitrogen gas to a negative pressure of 17 kPa with an immediate temperature ramp to 65 °C. Lastly, the ILG solution was left in the oven to polymerize for a minimum of 6 h. After polymerization, the ILG was stored in a desiccator at room temperature to minimize the absorption of atmospheric moisture.

ATR-FTIR Spectroscopy. The fractional conversion of C═C was determined using a Nicolet Magna-IR 560 FTIR Spectrometer in attenuated total reflectance (ATR) mode. A Gateway ATR 550 μL thermostabilized top-plate fitted with a ZnSe crystal (45°, 77 mm (longer length) × 63 mm (shorter length) x 10 mm × 6.0 mm) was utilized. In addition, a 1.0 mm thick rubber gasket was placed between the crystal and the heating block to ensure an adequate seal. The top-plate was maintained at 65 °C using circulated water as the heating medium. After collection of a spectral background and basis vectors, the ILG resin was injected into the cavity between the crystal and the heating block using existing ports on the top-plate. Spectra were taken in approximately one minute intervals for 20 h.

Using KBr salt pellets with a diameter of 13.05 mm and a thickness of 0.85 mm, FTIR spectroscopy in transmission mode was used to obtain neat spectra of AMPS and MBA.

In order to follow peak behavior more clearly, peak fitting was performed in OriginPro 8 (OriginLab Corp.) using the Peak Analyzer analysis tool whereby a baseline was generated and subsequently

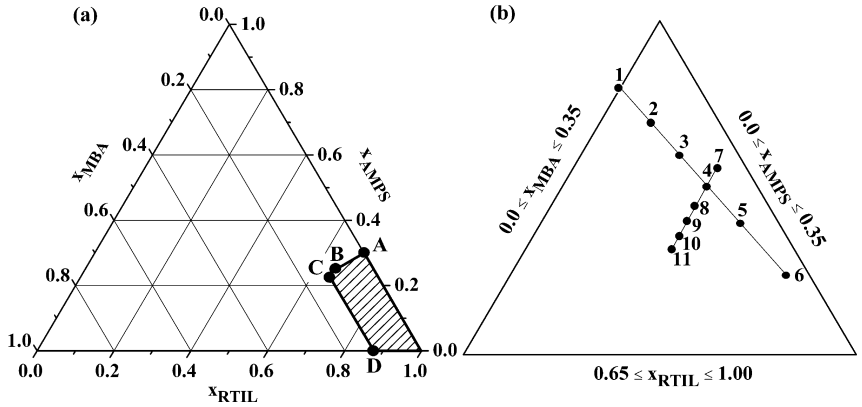

Figure 1. AMPS:MBA:[EMIM][EtSO$_4$] ternary plots with the monomer solubility window in the temperature range of 25 to 65 °C indicated by the dashed region on ternary plot (a). Ternary plot (b) is a magnification of the monomer solubility window that contains ILGs 1−6 (x_{MBA}:x_{AMPS} held constant) and ILGs 7−11 (x_{RTIL} held constant).

dx.doi.org/10.1021/am301777h | ACS Appl. Mater. Interfaces 2012, 4, 6142−6150

subtracted from the data (baseline created using adjacent-averaging to determine anchor points and a spline interpolation method), peak maxima were selected, and a fitting routine was applied to the data using a Gaussian−Lorentzian cross function with a 1.0×10^{-6} tolerance (χ^2) and parameters auto-initialized.

Immediately after curing in the spectrometer, a portion of the ILG was tested using a TA Q1000 differential scanning calorimeter (DSC) where a temperature sweep from 25 to 150 °C at 1.0 °C/min was conducted to detect any residual curing.

SEM Micrographs. A FEI Nova NanoSEM 600 scanning electron microscope was used to obtain surface morphology micrographs of the ILGs at ambient temperature and low vacuum. A Hitachi S-4700 SEM with an Energy Dispersive Spectrometer (EDAX) was used to chemically label artifacts seen during scanning.

Dynamic Mechanical Analysis (DMA). Dynamic mechanical analysis was performed on the ILGs (approximate dimensions: 35 mm × 12 mm × 4.0 mm) using a TA Instruments Q800 DMA in multifrequency strain mode with a dual-cantilever clamp. The temperature was ramped from room temperature to −90 °C at a cooling rate of 2.0 °C/min, held isothermally for 5 min, and then ramped to 0.0 °C at a heating rate of 2.0 °C/min. The frequency and amplitude of oscillation were maintained at 1.0 Hz and 7.5 μm, respectively. The glass transition temperature of the ILGs ($T_{g,ILG}$) was determined as the temperature corresponding to the maximum of the tan δ upon heating.[15,16] A slow cool down rate was needed as the ILGs were prone to fracturing upon rapid cooling. Due to the cracking issue, $T_{g,ILG}$ values were taken from the best of three runs with no averaging.

Mechanical Testing. The elastic modulus in compression (E_C) of the ILGs was obtained using an Instron 8871 in compression mode. Experiments were conducted according to the compression test at specified deflection method outlined in ASTM D695−02a for cylindrically shaped specimens with roughly a 2:1 diameter to height ratio.[17] Olive oil was utilized as a lubricant to reduce sample barreling during testing. An average displacement rate of 0.5 mm/min was utilized to ensure quasi-static mechanical testing. E_C was determined from the initial, linear slope of the compressive stress versus compressive strain curve immediately after the settling period.[18,19] Three specimens of each ILG were measured with the average E_C reported with standard deviations.

Gravimetric Analysis in [EMIM][EtSO$_4$]. Gravimetric analysis of ILGs immersed in moisture free [EMIM][EtSO$_4$] was conducted using rectangular-shaped specimens with an initial average mass of 240 mg. Three specimens of each sample were immersed in [EMIM][EtSO$_4$] in individual glass vials. The vials were placed in a nitrogen purged 60 °C oven. The specimens were weighed daily for 8.5 days. Reported are average values of the volume fractions of polymer in the swollen gel at equilibrium (φ_{2s}) with standard deviations.

Conductivity Measurements. Conductivity of the ILGs was determined by an electrochemical impedance spectroscopy technique that has been describe elsewhere.[20,21] The electrical conductivity was calculated using eq 1.

$$\sigma = \frac{1}{R}\left(\frac{l}{A_c}\right) \quad (1)$$

In eq 1, σ is the electrical conductivity in mS cm^{-1}, R is the bulk electrical resistance in mΩ, l is the ILG thickness in cm, and A_c is the ILG cross-sectional area in cm^2. Multiple specimens of each ILG were measured. Reported are average σ values with standard deviations.

RESULTS AND DISCUSSION

Cure Kinetics. The formation of oligomers, which could occur upon extensive heating of vinyl bonds, in solution prior to polymerization is assumed to be negligible. Free radical polymerization is dependent upon the formation of an active species that can propagate through the monomer repeat unit. Such an occurrence is dependent on monomer(s)−solvent interactions, and the presence of an initiating species. Autopolymerization is a rare occurrence that is specific to certain monomers. For example, styrene provides one of the few classic examples where autopolymerization occurs through a Diels−Alder reaction.[22,23] Acrylates and acrylamides are not known to undergo autopolymerizations under the reaction conditions utilized in this study.[24] The strong dipole moment present in [EMIM][EtSO$_4$], the nonexistence of all initiating species, including oxygen, and stability of the monomers utilized results in a low probability of transformation of monomer vinyl bonds into oligomer or polymer-sized molecules during the elevated temperature dissolution stage of the synthesis.

An FTIR method developed and described by Brill and Palmese was used to monitor the depletion of C═C of AMPS and MBA during cure.[25] Figure 2 shows transmission spectra of

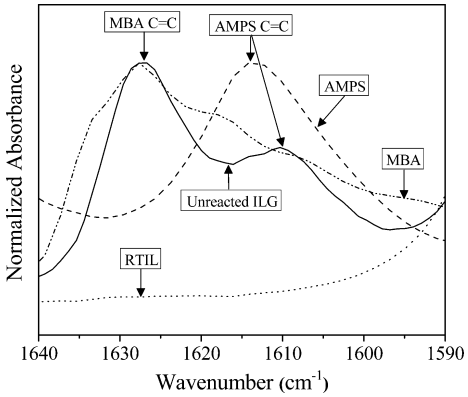

Figure 2. Spectra of neat AMPS, MBA, RTIL, and their combination prior to *in situ* polymerization.

both AMPS and MBA as well as ATR spectra of [EMIM][EtSO$_4$] and unreacted ILG solution from 1640 to 1590 cm^{-1}. According to the overlaying peak pattern, the peaks at 1628 and 1611 cm^{-1} correspond to the stretching of the terminal vinyl bonds of MBA and AMPS, respectively. These peaks were monitored independently during cure to follow the reaction kinetics. The [EMIM][EtSO$_4$] spectrum appropriately lacks any aliphatic vinyl peaks. There exists overtones in the MBA spectra; however, this phenomenon was excluded from the fractional conversion analysis but is noted here. To correct for absorbance intensity changes due to physical changes during cure, such as sample thickness, we monitored the broad absorption intensity corresponding to the stretching of secondary amine bonds in both AMPS and MBA at 3300 cm^{-1} and utilized it as a correction factor (not shown in Figure 2).

Figure 3 depicts a representative spectral series obtained via ATR-FTIR spectroscopy during 65 °C *in situ* cure of ILG-4 (Figure 1). Due to maintaining a constant mole ratio of PPS to C═C for the synthesis of the ILGs and adhering to a minimum of 6 h for curing, the kinetic analysis of ILG-4 is assumed to, in general, represent the overall kinetic behavior of the ILGs.

During these experiments, the full mid-IR spectral range was obtained; however, the overlapping vinyl peak region between 1628 and 1611 cm^{-1} is of particular interest. In Figure 3, the overall peak area decreases as cure time increases and essentially vanishes after 300 min (5 h). This decrease and eventual disappearance of the vinyl peak range provides a qualitative assessment that both AMPS and MBA monomers polymerize to near completion in the presence of [EMIM][EtSO$_4$].

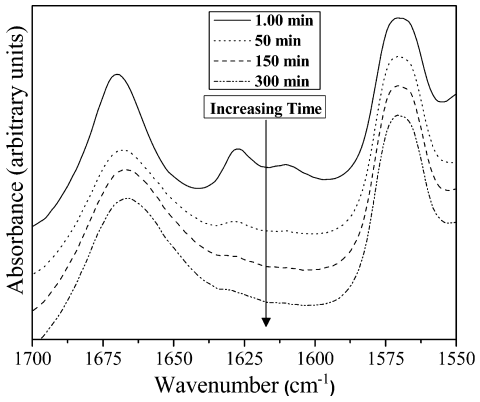

Figure 3. Representative spectral series obtained via *in situ* ATR-FTIR spectroscopy during polymerization of ILG formulation 4. Spectra were offset for clarity.

From the FTIR absorption data, eqs 2a and 2b were used to calculate the normalized fractional conversion of AMPS and MBA C═C to polymeric C−C.[25]

$$\alpha_{\mathrm{AMPS,C=C}}(t) = 1 - \left(\frac{\mathrm{ABS}(t)_{1611\mathrm{cm}^{-1}}}{\mathrm{ABS}(t=0)_{1611\mathrm{cm}^{-1}}}\right)\left(\frac{\mathrm{ABS}(t=0)_{3300\mathrm{cm}^{-1}}}{\mathrm{ABS}(t)_{3300\mathrm{cm}^{-1}}}\right) \quad (2a)$$

$$\alpha_{\mathrm{MBA,C=C}}(t) = 1 - \left(\frac{\mathrm{ABS}(t)_{1628\mathrm{cm}^{-1}}}{\mathrm{ABS}(t=0)_{1628\mathrm{cm}^{-1}}}\right)\left(\frac{\mathrm{ABS}(t=0)_{3300\mathrm{cm}^{-1}}}{\mathrm{ABS}(t)_{3300\mathrm{cm}^{-1}}}\right) \quad (2b)$$

In eqs 2a and 2b, $\alpha_{C=C}$ is the fractional conversion of C═C for each monomer at time t and *ABS* is the absorption intensity of the peaks at time t. The peak areas and heights were determined by peak fitting knowing the behavior of the individual spectra of AMPS and MBA (Figure 4). The magnitude of the relevant peak heights were measured taking into account slight variations in the baseline. Additionally, for simplicity, the peak fitting did not take into account the overtones produced by the MBA vinyl bonds, and therefore, the absorbance intensity at 1611 cm^{-1} is combined into one peak fit.

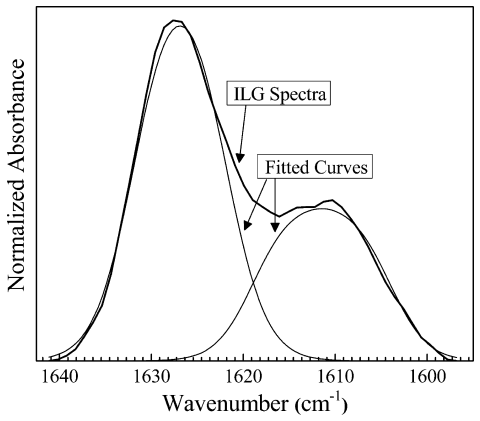

Figure 4. Peak fitting of a representative ILG spectrum prior to curing showing two vibrational frequencies between 1640 and 1595 cm^{-1}. Absorption peaks appear at 1628 cm^{-1} for C═C in MBA and 1611 cm^{-1} for C═C in AMPS. The C═C overtones from MBA have been ignored.

A modified version of Kamal's empirical model by Lam et al. that captures the isothermal cure behavior of thermosetting resins which exhibit autocatalytic behavior was fitted to the ATR-FTIR conversion data to estimate a polymerization rate constant and reaction order (eqs 3 and 4).[25−28]

$$\frac{d\alpha_t}{dt} = k\alpha_t^m(\alpha_u - \alpha_t)^{2-m} \quad (3)$$

$$\alpha_t = \frac{\alpha_u[kt\alpha_u(1-m)]^{1/1-m}}{1 + [kt\alpha_u(1-m)]^{1/1-m}} \quad (4)$$

In eqs 3 and 4, α_t is the fractional conversion at time t, α_u is the ultimate fractional conversion at $t = t_{final}$, k is the reaction rate constant, and m is the reaction order.

Figure 5 shows the fractional conversion data as a function of time for AMPS and MBA and the corresponding model fits.

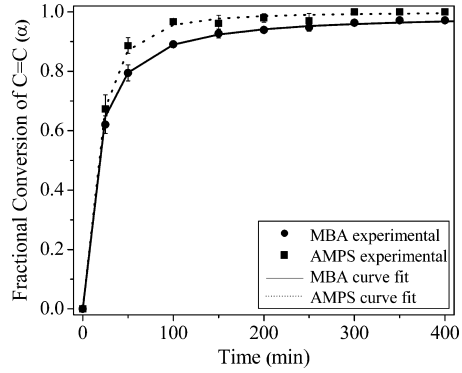

Figure 5. Average fractional conversion (α) of C═C as a function of time with curve fits for ILG formulation 4 at a cure temperature of 65 °C.

95% plus cure was achieved for both AMPS and MBA in about 300 min. In applying the empirical model to the acquired data, the average k and m were calculated to be 0.105 min^{-1} and 0.079 min^{-1} and 0.411 and 0.093 for AMPS and MBA, respectively. These values are on the same order of magnitude of reported literature values for traditional free radical polymerization kinetics.[26] The average error between the experimental data and model fits was fairly insignificant at 9.8 × 10^{-4} and 4.4 × 10^{-5} for AMPS and MBA, respectively.

AMPS has a slightly higher rate constant than MBA, a difference that is greater than the error. In comparing the two monomers, both have acrylamide functional groups that exhibit resonance stabilization. However, AMPS has a sulfonic acid substituent that is electron withdrawing. This phenomenon may influence the reactivity of the vinyl group but the interaction of the sulfonic acid with [EMIM][$EtSO_4$] may have an even greater effect. This interaction may form ionic clusters or ionic aggregates throughout the gel that, in turn, may influence the overall cure kinetics.[29−32] An overall increase in the reaction rate for polymerizations in RTILs compared to traditional solvents has been reported in the literature.[3,33,34] Harrison et al. attributes this enhancement to the presence of the RTIL causing a decrease in the activation energy of propagation.[33] This decrease is due to an increased polarity of the solvent medium that allows for an increased contribution of

dx.doi.org/10.1021/am301777h | ACS Appl. Mater. Interfaces 2012, 4, 6142−6150

Table 1. ILG Formulations from Figure 1 with Physical Property Results

plot no.	x_{MBA}/x_{AMPS}	x_{RTIL}	$T_{g,ILG}$ (°C)[a]	E_C (k Pa)	Log M_C (g mol^{-1})[b]	φ_{2s}[c]	χ[d]	σ (mS cm^{-1})[e]
1	0.36	0.68	−49.1	5226 ± 144	3.07	0.27	0.48	0.52
2	0.36	0.71	−52.7	3694 ± 133	3.2	0.24	0.5	0.35
3	0.36	0.76	−52.9	2073 ± 62	3.43	0.2	0.52	0.71
4	0.36	0.8	−55.3	432 ± 45	4.08	0.16	0.55	0.51
5	0.36	0.85	−59.2	203 ± 8.0	4.37	0.11	0.53	2.14
6	0.36	0.9	−64.6	≤200[f]	–	0.06	1.19	
7	0.2	0.8	−53.5	240 ± 42	4.33	0.11	0.52	1.79
4	0.36	0.8	−55.3	432 ± 45	4.08	0.16	0.55	0.51
8	0.5	0.8	−61.6	1801 ± 162	3.46	0.18	0.52	1.45
9	0.6	0.8	−62.6	3005 ± 315	3.24	0.27	0.48	1.07
10	0.8	0.8	−66.5	6602 ± 403		0.19		1
11	1.1	0.8	−66.9	3290[g]		0.18[g]		1.09

[a]Because of cracking at low temperatures, $T_{g,ILG}$ values were taken from the best of three runs with no averaging. [b]Maximum standard deviation = ±0.08. [c]Maximum standard deviation = ±0.003. [d]Maximum standard deviation = ±0.006. [e]Maximum standard deviation = ±0.28. [f]Value within the error of load cell. Approximate value reported to show general trend. [g]Contained regions of undissolved PPS that altered the integrity of the ILG; see the following discussions.

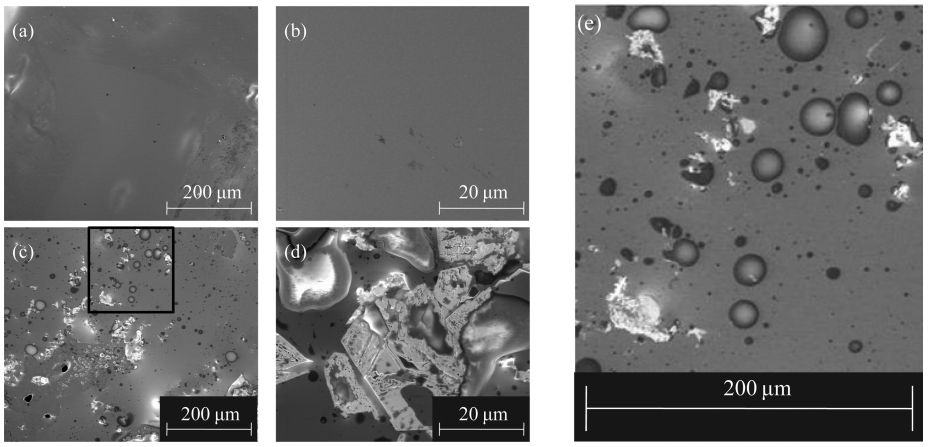

Figure 6. SEM micrographs of ILG formulations (a, b) 7 and (c−e) 11, of which e is an enlargement of the boxed region in c.

charge-transfer structures to the transition state.[33] An alternative explanation is the "bootstrap" effect, which is caused by poor solvation of the cross-linked polymer network. This leads to either an increase in local monomer concentration around the radical active sites or the formation of radical-solvent or monomer−solvent complexes that exhibit enhanced reactivity.[33] The [EMIM][$EtSO_4$]-AMPS ionic interaction may further decrease the activation energy of propagation or enhance the radical−solvent or monomer−solvent complexes for the AMPS monomer; thereby, producing a slightly higher reaction rate compared to MBA.

DSC was used to verify conversion immediately following the ATF-FTIR cure study experiments. Results contained a minimal residual exotherm indicating that most of the reaction took place while in the FTIR, hence verifying the spectroscopy data.

To confirm the above assumption that the kinetics analysis of ILG-4 represents the kinetics for all the formulations, ATR-FTIR spectra were obtained of each ILG after cure. All spectra mimicked the 300 min spectrum in Figure 3, thus validating our assumption.

Physical Property Results. Table 1 summarizes the $T_{g,ILG}$, E_C, σ, M_C, φ_{2s}, and χ for all of the eleven ILG formulations illustrated in Figure 1. The table is divided into two sections. The upper section contains ILGs that have a constant x_{MBA}:x_{AMPS} while varying x_{RTIL}. The lower section contains ILGs that have a constant x_{RTIL} while varying x_{MBA}:x_{AMPS}.

SEM Results. Figure 6 shows SEM micrographs for ILG-7 and ILG-11. The micrographs of ILG-7, images a and b in Figure 6, are relatively uniform, show no crystalline regimes or apparent regions of polymer-[EMIM][$EtSO_4$] phase separation at the micrometer length scale. Image a, however, contains a few bright protrusions and dark circles as well as a relatively rough region in the lower right corner. These characteristics are a result of mechanical shearing and tearing of the ILG during sample preparation. Image b contains a few of these shearing defects but, overall, is relatively uniform. SEM micrographs of ILG formulations 1−2, 4, and 8−11 were also obtained of which formulations 1−2, 4, and 8−9 showed similar results to ILG-7.

The micrographs of ILG-11, images c−e in Figure 6, on the other hand, show significant crystallinity, shearing defects, which are a result of sample prep, and possible regions of polymer-[EMIM][$EtSO_4$] phase separation. Image e is an enlargement of the boxed region in image c. The crystalline regions in these images were identified, via EDAX, to contain high concentrations of potassium and sulfur indicating the likely presence of undissolved PPS. The presence of small regions of undissolved PPS is most likely a result of the significantly higher viscosity of these precured resins compared

to the other formulations, which resulted in not achieving uniform dispersion and complete dissolution of crystalline PPS. However, as the cure kinetics analysis showed, 95% plus cure was still achieved. Additionally, in image e, relatively symmetric "bubbles" exist that contain a bright core with a dark outer region. These bubbles represent possible solvent phase separation from the polymer network. This phenomenon along with the undissolved PPS, as demonstrated in the following analyses, produces ILGs with physical properties that deviate from the observed trends. The SEM micrographs of ILG-10 also exhibited undissolved PPS crystals and possible phase separation regions but to a lesser visible extent than ILG-11. As a result, ILG-10 and ILG-11 are included in the following analysis for completeness but are often excluded from the observed general trends.

Thermomechanical Analysis. In Table 1, at constant x_{MBA}:x_{AMPS}, $T_{g,ILG}$ decreases as x_{RTIL} increases. $T_{g,ILG}$ also decreases as x_{RTIL} is held constant and x_{MBA}:x_{AMPS} increases. To gain a qualitative insight into the trends of the experimental data, a direct comparison can be made with the theoretical T_g values predicted by the Fox equation (eq 5).[35]

$$\frac{1}{T_{g,ILG}} = \frac{w_{RTIL}}{T_{g,RTIL}} + \frac{w_{polymer\ network}}{T_{g,polymer\ network}} \quad (5)$$

In eq 5, w_{RTIL} is the mass fraction of RTIL, $w_{polymer\ network}$ is the mass fraction of the AMPS-MBA polymer network in the ILG, and $T_{g,RTIL}$, $T_{g,polymer\ network}$, and $T_{g,ILG}$ are the T_g values, in Kelvin, of [EMIM][$EtSO_4$], the AMPS-MBA polymer network, and the ILG, respectively. $T_{g,RTIL}$ = 193.8 K (−79.4 °C), which is an average value of reported literature data, was used.[36,37] The values used for $T_{g,polymer\ network}$ were obtained from DSC after subjecting ILGs to a solvent exchange with water and then heating under vacuum; thus, extracting the [EMIM][$EtSO_4$]. To avoid confusion by the reader, the determination of $T_{g,polymer\ network}$ was completed prior to finalizing the ILG formulations outlined in Table 1. The prior formulations actually encompassed a slightly broader range within the solubility window (Figure 1). Therefore, $T_{g,polymer\ network}$ values used for the ILG formulations listed in Table 1 were derived by extrapolating a polynomial fit of our prior experimental data from a plot of $T_{g,polymer\ network}$ versus x_{MBA}:x_{AMPS}.

In Figure 7, $T_{g,ILG}$ decreases with x_{RTIL}. While holding x_{MBA}:x_{AMPS} constant, increasing the concentration of plasticizer produces a rubbery gel with a lower T_g; a T_g that approaches the T_g of pure plasticizer. [EMIM][$EtSO_4$] and AMPS are a nontraditional plasticizer and monomer, respectively, that exhibit strong ionic character. [EMIM][$EtSO_4$] has potential to interact with the cross-linked polymer network through ionic bonding with the sulfonic acid moiety located on the AMPS. Moreover, the formation of ionic aggregates or ionic clusters during polymerization, thus resulting in the formation of heterogeneous network structures, is possible as described in other studies.[29−32] Therefore, it was anticipated that this ionic character of the ILGs would greatly influence the long-range cooperative motions of the cross-linked polymer network. However, the $T_{g,ILG}$ values predicted by the Fox equation are in good agreement (standard deviation of the model errors = 5.57) with the experimental values indicating that the concentration of the plasticizing agent and not the ionic character of the ILGs has a larger effect on the long-range cooperative motions of the polymer network, as the Fox equation assumes perfect miscibility.[9] To gain a deeper understanding of the ILGs and the mobility of the polymer networks, we recommend multifrequency DMA experiments as future work.

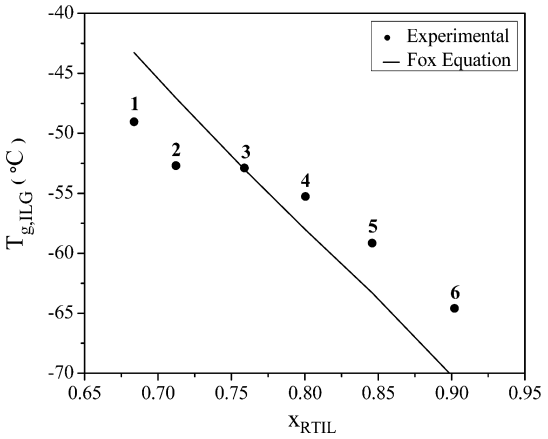

Figure 7. $T_{g,ILG}$ as a function of x_{RTIL} where x_{MBA}:x_{AMPS} is held constant at 0.36. Experimental measurements were taken using DMA while the Fox equation fit was derived using $T_{g,polymernetwork}$ (obtained from DSC data) and $T_{g,RTIL}$ (average of literature values).[36,37] Experimental data shown are the best of three runs.

Referring to the lower portion of Table 1, the experimental $T_{g,ILG}$ values decrease with increasing x_{MBA}:x_{AMPS} while holding x_{RTIL} constant. On the other hand, the predicted Fox equation $T_{g,ILG}$ values, not shown, increase. In theory by adding more MBA, the cross-link density should increase, which should in turn increase T_g. However, the experimental $T_{g,ILG}$ values exhibit the opposite trend. ILG-10 and ILG-11 most likely skew the results because of these ILGs containing a high concentration of undissolved PPS and possible phase separated regions. In spite of this observation, an increase in x_{MBA}:x_{AMPS} while holding x_{RTIL} constant results in more MBA present. By increasing x_{MBA}, the interaction between the ionic character of the polymer network and the [EMIM][$EtSO_4$] decreases. Because of the existence of ions in the ILGs, the presence of physical cross-links between the solvent and the polymer network are possible. Thus, MBA may act as a plasticizer with respect to physical cross-linking, thereby, lowering the $T_{g,ILG}$.

$T_{g,ILG}$ values of all the ILGs are within a 20 °C range with values not far from the T_g of pure RTIL (Table 1). This is a result of all the ILGs containing a relatively high concentration of plasticizing agent. This signifies that the concentration of [EMIM][$EtSO_4$] within the monomer solubility window of Figure 1 dominates $T_{g,ILG}$.

Compressive Modulus. E_C values tabulated in Table 1 are plotted as a function of x_{RTIL} (x_{MBA}:x_{AMPS} is held constant) and as a function of x_{MBA}:x_{AMPS} (x_{RTIL} is held constant) in Figures 8 and 9, respectively. In Figure 8, E_C decreases with increasing x_{RTIL} at constant x_{MBA}:x_{AMPS}. An increase in plasticizer concentration, an inherently weak mechanical performer, reduces the overall concentration of cross-linked polymer within ILG per unit volume due to swelling effects, thus decreasing mechanical performance.

In Figure 9, E_C increases with increasing x_{MBA}:x_{AMPS} at constant x_{RTIL} up to 0.8. By introducing an excess amount of AMPS, the spacing between the cross-linking bonds increases, on average, producing a more compliant polymer structure with greater conformational freedom; thus, decreasing E_C. ILG-11 deviates from the general trend observed due to containing a small fraction of undissolved PPS and possible regions of phase

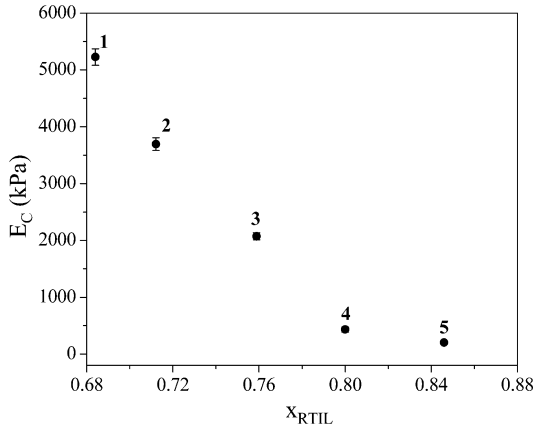

Figure 8. E_C as a function of x_{RTIL} where x_{MBA}:x_{AMPS} is held constant at 0.36.

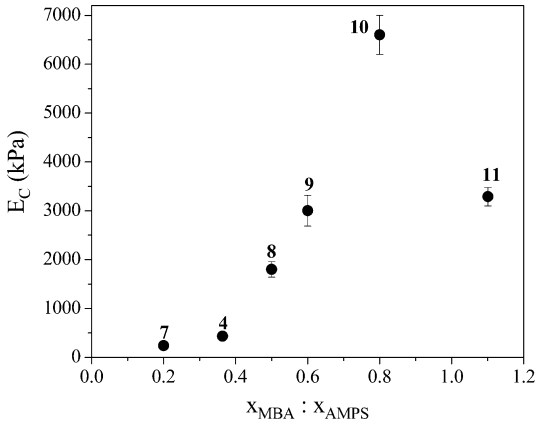

Figure 9. E_C as a function of x_{MBA}:x_{AMPS} where x_{RTIL} is held constant at 0.80.

separation. These attributes may have affected the homogeneity of the ILG and could have decreased the effective cross-link density, thus decreasing E_C.

Gravimetric Analysis in [EMIM][EtSO$_4$]. The purpose of this portion of the study was to obtain insight into the swelling behavior of the ILGs and to calculate χ for each ILG. The experiments were conducted at an elevated temperature to shorten the studies duration with daily weight measurements occurring at ambient conditions. Moreover, the gravimetric analysis assumes that [EMIM][EtSO$_4$] is the only component being transferred and that the presence of atmospheric water vapor is negligible.

Figure 10 shows the swelling behavior of the ILGs on a ternary diagram with vectors that depict the magnitude and direction of [EMIM][EtSO$_4$] swelling. Also included in the ternary diagram is a dashed line that separates the ILGs that swelled in excess [EMIM][EtSO$_4$] from those that apparently leeched solvent. One explanation for the leeching of solvent suggests that these ILGs were already saturated with [EMIM]-[EtSO$_4$] and any excess RTIL present in the gels prefers to be in the pure, liquid phase rather than the polymer phase. Leeching of [EMIM][EtSO$_4$] was observed to occur at x_{MBA}:$x_{AMPS} \geq 0.5$. As the molecular weight between cross-links decreases, a stiff, tightly packed cross-linked polymer network is produced. This results in a severe reduction of molecular conformations and an increase in gel stiffness, which

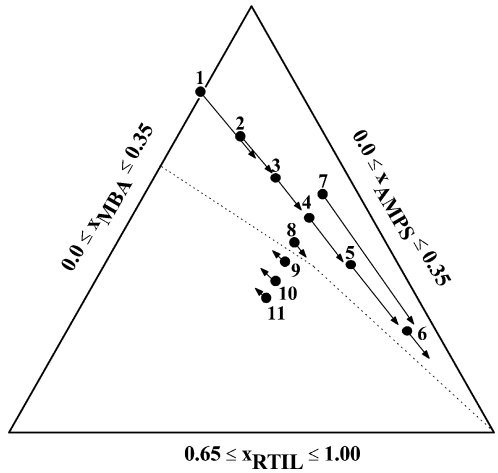

Figure 10. Magnified AMPS:MBA: [EMIM][EtSO$_4$] ternary plot with ILG formulations. The black arrows are vectors representing the equilibrium [EMIM][EtSO$_4$] shift and the dashed line separates formulations that swelled from those that deswelled.

limits solvent uptake. The reverse can be stated for ILGs that swelled in excess [EMIM][EtSO$_4$].

An alternative explanation is related to ILG-10 and ILG-11 containing undissolved PPS. When the ILG is exposed to excess solvent, any component not attached to the network, i.e., undissolved PPS, has the ability to transfer out of the gel; consequently, nullifying the key assumption that [EMIM]-[EtSO$_4$] was the only component exchanged in the swelling experiments. Possible phase separation would also enhance the deswelling of an ILG.

ILG-10 and ILG-11 have been excluded from the M_C and χ calculations since the following calculations utilized equations only applicable to homogeneous systems.

The possibility of deficient mixing due to high solution viscosity or possible phase separation is not ruled out for ILG-9, even though the SEM analysis did not reveal such phenomena.

Interaction Parameter. E_C values can be used with eq 6 to calculate the apparent molecular weight between cross-links, M_C.[38] In eq 6, ρ is the density of the ILG, R is the universal gas constant, T is the temperature in Kelvin, ν_2 is the volume fraction of polymer in the gel, E_C is the elastic modulus in compression, and $\bar{r}_i^2/\bar{r}_o^2$ is the front factor and is assumed to be equal to unity. The density of the ILG is estimated to be about 1.2 g cm^{-3}, with the gas constant and temperature equal to 8.314 Pa m^3 mol^{-1} K^{-1} and 298 K, respectively. The density of the polymer network is assumed to be approximately equal to the density of [EMIM][EtSO$_4$]; therefore, the mass fraction of polymer is equal to the volume fraction of the polymer in the ILGs. Average M_Cs with standard deviations are shown in Table 1.

$$M_C \cong \frac{3\rho RT\nu_2^{1/3}}{E_C}\frac{\bar{r}_i^2}{\bar{r}_o^2} \quad (6)$$

Assuming that the final measured weights in the gravimetric study represent the equilibrium swelling behavior for each ILG, χ can be calculated using a modified and rearranged form of the Bray and Merrill equation, eq 7, along with the calculated M_Cs.[39,40] In eq 7, φ_{2s} is the volume fraction of polymer in the swollen gel at equilibrium, φ_{2r} is the volume fraction of polymer in the relaxed or before exposure to excess [EMIM][EtSO$_4$] state, M_C is the apparent molecular weight between cross-links,

ν_{sp} is the specific volume of the polymer network, and V_1 is the molar volume of the solvent. In studies of polymer networks that were formed in the wet state, i.e., in the presence of solvent, and then subjected to additional solvent in swelling experiments, Bray and Merrill modified their original equation to exclude M_n. However, both forms of the equation were derived using Flory's network structure description for dense networks. In order to account for the solvent present initially in the polymer network, thereby creating a less dense network, Raman incorporated the initial solvent volume in $\varphi_{2r.}$[39] This further modified version of the Bray and Merrill equation is eq 7. The specific volume of the polymer network is assumed to be 0.909 $cm^3\ g^{-1}$ and the molar volume of [EMIM][$EtSO_4$] was calculated to be 19.56 $cm^3\ mol^{-1}$. Because othe densities of the [EMIM][$EtSO_4$] and the polymer network are very similar, the mass fraction of the polymer network is assumed to be equal to the volume fraction of the polymer network in the ILG.

$$\chi = -\left\{\left(\frac{V_1\phi_{2r}^2}{\upsilon_{sp}M_C}\right)\left[\left(\frac{\phi_{2s}}{\phi_{2r}}\right)^{1/3} - \frac{1}{2}\left(\frac{\phi_{2s}}{\phi_{2r}}\right)\right] + \ln(1-\phi_{2s}) + \phi_{2s}\right\}\left(\frac{1}{\phi_{2s}^2}\right) \quad (7)$$

The χ values along with the φ_{2s} values are tabulated in Table 1. The calculated χ values fall within the range of typical values of polymer−liquid interaction parameters reported in the literature.[38,41]

χ remains relatively constant and slightly positive (Table 1). Even though the χs are positive, favorable entropic forces and possible diffusion limitations induced by the cross-linked polymer network seem to outweigh unfavorable enthalpy of mixing or potential repulsive polymer−solvent interactions. Thus, miscibility is favored. Focusing on the lower portion of Table 1, χ was anticipated to increase with increasing x_{MBA} because of the decrease in M_C. However, instead of the addition of MBA producing an overall tighter network structure, MBA decreases the physical cross-links produced by the ionic interaction between the polymer network and [EMIM][$EtSO_4$] and acts as a promoter for favorable mixing.

Conductivity Analysis. σ of pure [EMIM][$EtSO_4$] has been reported to be 3.76 mS cm^{-1}.[42] The σ values reported in Table 1 are interesting and useful; however, a higher conductivity, presumably proton conductivity, results when a similar system is swollen in water.[43] This polymer system uses AMPS and a vinyl ester resin based on a catalyzed methacrylated 4,4' diglycidyl ether of bisphenol A, instead of MBA, as the cross-linking agent. Rahmathullah has reported conductivities in the range of 1.00 mS cm^{-1} to 27 mS cm^{-1}, which has a considerably higher maximum than the conductivities for the ILGs.[14,43]

σ values of all the ILGs are less than that of pure RTIL indicating that the polymer network hinders proton transfer and the ILGs are considered to be relatively poor ion conductors compared to hydrogels. However, this does not preclude the potential usefulness of the ILGs in other applications, such as separation membranes.

CONCLUSIONS

In conclusion, ionic liquid gels were generated via a free radical copolymerization of 2-acrylamido-2-methyl-1-propanesulfonic acid and *N,N'*-methylenebis(acrylamide) using 1-ethyl-3-methylimidazolium ethylsulfate as a room temperature ionic liquid solvent medium. Chemical cross-linking, ionic induced physical cross-links between the polymer network and [EMIM][$EtSO_4$], and the chemical composition influenced the physical properties of the ILGs with all ILGs in the rubbery state at room temperature. The conductivities of the ILGs were less than that of pure [EMIM][$EtSO_4$]; however, based on the material properties, the ILGs express potential as membranes for separations. Moreover, ILGs express potential as tissue surrogates for ballistic testing due to the mechanical properties of the ILGs being similar to those of collagen-based ballistic gelatin and to the greater environmental stability of the ILGs compared to ballistic gelatin (data not shown).[44]

AUTHOR INFORMATION

Corresponding Author

§Tel: (215) 895-5814. Fax: (215) 895-5837. E-mail: palmese@coe.drexel.edu.

Present Addresses

‡University of Delaware, Department of Chemical & Biomolecular Engineering and Center for Composite Materials, Newark, DE 19716

⊥California Polytechnic State University, Department of Chemistry & Biochemistry, San Luis Obispo, CA 93407

Notes

The authors declare no competing financial interest.

ACKNOWLEDGMENTS

The authors from Drexel University acknowledge the U.S. Army Research Laboratory for financial support under the Army Materials Center of Excellence Program, Contract W911NF-06-2-0013. J.F.S. was also supported in part by an appointment to the Research Participation Program at the U.S. Army Research Laboratory administered by the Oak Ridge Institute for Science and Education through an interagency agreement between the U.S. Department of Energy and US-ARL. P.J.C. was, by an appointment to the Research Participation Program, at the U.S. Army Research Laboratory administered by the National Research Council through an interagency agreement between the U.S. Department of Energy and US-ARL. J.F.S. also acknowledges Mr. Andres Bujanda at ARL for his assistance with mechanical testing and SEM imaging.

REFERENCES

(1) Ueki, T.; Watanabe, M. *Macromolecules* **2008**, *41*, 3739−3749.

(2) Huddleston, J. G.; Visser, A. E.; Reichert, W. M.; Willauer, H. D.; Broker, G. A.; Rogers, R. D. *Green Chem.* **2001**, *3*, 156−164.

(3) Hong, K.; Zhang, H.; Mays, J. W.; Visser, A. E.; Brazel, C. S.; Holbrey, J. D.; Matthew, W. M.; Rogers, R. D. *Chem. Commun.* **2002**, *13*, 1368−1369.

(4) Li, Z.; Jiang, J.; Lei, G.; Gao, D. *Polym. Adv. Technol.* **2006**, *17*, 604−607.

(5) Strehmel, V.; Laschewsky, A.; Wetzel, H.; Gornitz, E. *Macromolecules* **2006**, *39*, 923−930.

(6) Snedden, P.; Cooper, A. I.; Scott, K.; Winterton, N. *Macromolecules* **2003**, *36*, 4549−4556.

(7) Susan, M. A. B. H.; Kaneko, T.; Noda, A.; Watanabe, M. *J. Am. Chem. Soc.* **2005**, *127*, 4976−4983.

(8) Winterton, N. *J. Mater. Chem.* **2006**, *16*, 4281−4293.

(9) Matsumoto, K.; Endo, T. *Macromolecules* **2008**, *41*, 6981−6986.

(10) Dinu, M. V.; Ozmen, M. M.; Dragan, E. S.; Okay, O. *Polymer* **2007**, *48*, 195−204.

(11) Gong, J. P.; Katayama, Y.; Kurokawa, T.; Osada, Y. *Adv. Mater.* **2003**, *15*, 1155−1158.
(12) Ozmen, M. M.; Okay, O. *Polym. Bull.* **2004**, *52*, 83−90.
(13) Tanaka, Y.; Ping, J. P.; Osada, Y. *Prog. Polym. Sci.* **2005**, *30*, 1−9.
(14) Rahmathullah, M. A. M.; Snyder, J. D.; Elabd, Y. A.; Palmese, G. R. *J. Polym. Sci., Part B: Polym. Phys.* **2010**, *48*, 1245−1255.
(15) Ziaee, S.; Palmese, G. R. *J. Polym. Sci., Part B: Polym. Phys.* **1999**, *37*, 725−744.
(16) La Scala, J. J.; Orlicki, J. A.; Winston, C.; Robinette, E. J.; Sands, J. M.; Palmese, G. R. *Polymer* **2005**, *46*, 2908−2921.
(17) *ASTM D695 - 02a*; ASTM International: West Conshohocken, PA, 2002.
(18) Saunder, J. H.; Frisch, K. C. *Monographs on Plastics Vol. 1: Plastic Foams (In Two Parts): Part 1*; Marcel Dekker: New York, 1972.
(19) Dowling, N. E. *Mechanical Behavior of Materials (Engineering Methods for Deformation, Fracture, and Fatigue)*, 3rd ed.; Pearson Education: Upper Saddle River, NJ, 2007.
(20) DeLuca, N. W.; Elabd, Y. A. *J. Membr. Sci.* **2006**, *282*, 217−224.
(21) Hallinan, D. T.; Elabd, Y. A. *J. Phys. Chem. B* **2007**, *111*, 13221−13230.
(22) Flory, P. J. *J. Am. Chem. Soc.* **1937**, *59*, 241−253.
(23) Mayo, F. R. *J. Am. Chem. Soc.* **1968**, *90*, 1289−1295.
(24) Cameron, N. R.; Reid, A. J. *Macromolecules* **2002**, *35*, 9890−9895.
(25) Brill, R. P.; Palmese, G. R. *J. Appl. Polym. Sci.* **2000**, *76*, 1572−1582.
(26) Brill, R. P.; Palmese, G. R. *J. Appl. Polym. Sci.* **2006**, *101*, 2784−2792.
(27) Kamal, M. R.; Sourour, S. *Polym. Eng. Sci.* **1973**, *13*, 59−64.
(28) Lam, P. W. K.; Plaumann, H. P.; Tran, T. *J. Appl. Polym. Sci.* **1990**, *41*, 3043−3057.
(29) Eisenberg, A.; Hird, B.; Moore, R. B. *Macromolecules* **1990**, *23*, 4098−4107.
(30) Eisenberg, A.; Kim, J. S. *Introduction to Ionomers*; John Wiley & Sons: New York, 1998; pp 59−82, 244−263, 272−274.
(31) Eisenberg, A. *Macromolecules* **1970**, *3*, 147−154.
(32) Ma, X.; Sauer, J. A.; Hara, M. *Macromolecules* **1995**, *28*, 3953−3962.
(33) Harrisson, S.; Mackenzie, S. R.; Haddleton, D. M. *Macromolecules* **2003**, *36*, 5072−5075.
(34) Vygodskii, Y. S.; Mel'nik, O. A.; Lozinskaya, E. I.; Shaplov, A. S.; Malyshkina, I. A.; Gavrilova, N. D.; Lyssenko, K. A.; Antipin, M. Y.; Golovanov, D. G.; Korlyukov, A. A.; Ignat'ev, N.; Welz-Biermann, U. *Polym. Adv. Technol.* **2007**, *18*, 50−63.
(35) Shah, B. N.; Schall, C. A. *Thermochim. Acta* **2006**, *443*, 78−86.
(36) Fernandez, A.; Torrecilla, J. S.; Garcia, J.; Rodriguez, F. *J. Chem. Eng. Data* **2007**, *52*, 1979−1983.
(37) Zhang, Z.-H.; Tan, Z.-C.; Sun, L.-X.; Jia-Zhen, Y.; Lv, X.-C.; Shi, Q. *Thermochim. Acta* **2006**, *447*, 141−146.
(38) Sperling, L. H. *Introduction to Physical Polymer Science*, 4th ed.; John Wiley & Sons: Hoboken, NJ, 2006; pp 445−462.
(39) Raman, V. Design of Nanoporous Polymer Networks using a Reactive Encapsulation of Solvent (RES) Technique. *PhD Thesis*, Drexel University, Philadelphia, PA, 2005; pp 157−162.
(40) Bray, J. C.; Merrill, E. W. *J. Appl. Polym. Sci.* **1973**, *17*, 3779−3794.
(41) Barton, A. F. M. *CRC Handbook of Polymer−Liquid Interaction Parameters and Solubility Parameters: Part II*; CRC Press: Boca Raton, FL, 1990; p 178.
(42) MSDS - [EMIM][$EtSO_4$] - ECOENGTM212 (1-Ethyl-3-Methylimidazolium Ethylsulfate); 2006.
(43) Rahmathullah, M. A. Multifunctional Polymers via Incorporation of Ionic Groups at Molecular and Mesoscopic Length Scales. *PhD Thesis*, Drexel University, Philadelphia, PA, 2008; pp 106−108.
(44) Stanzione III, J. F. Characterization of Room-Temperature Ionic Liquid Solvent-Based, Free Radical Copolymerized Network Gels. *PhD Thesis*, Drexel University, Philadelphia, PA, 2008; pp 111−113.